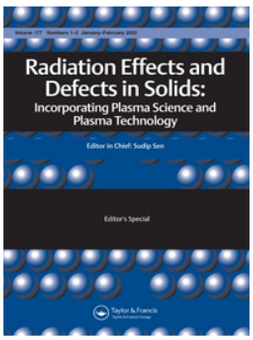

Taylor & Francis
Taylor & Francis Group

Radiation Effects and Defects in Solids

Incorporating Plasma Science and Plasma Technology

ISSN: (Print) (Online) Journal homepage: https://www.tandfonline.com/loi/grad20

Breakup of transport barriers in plasmas with flow described by symplectic maps

Carolina A. Tafoya & Julio J. Martinell

To cite this article: Carolina A. Tafoya & Julio J. Martinell (2022) Breakup of transport barriers in plasmas with flow described by symplectic maps, Radiation Effects and Defects in Solids, 177:1-2, 124-136, DOI: 10.1080/10420150.2022.2049787

To link to this article: https://doi.org/10.1080/10420150.2022.2049787

Published online: 17 Mar 2022.

RADIATION EFFECTS & DEFECTS IN SOLIDS
2022, VOL. 177, NOS. 1–2, 124–136
https://doi.org/10.1080/10420150.2022.2049787

Taylor & Francis
Taylor & Francis Group

Breakup of transport barriers in plasmas with flow described by symplectic maps

Carolina A. Tafoya and Julio J. Martinell

Instituto de Ciencias Nucleares, UNAM, México D.F., Mexico

ABSTRACT

Transport barriers associated with the last KAM surfaces to break up are studied in the context of turbulent transport produced by a discrete spectrum of waves in two dimensions using a 2D symplectic map. It is based on the guiding center motion of test particles but finite Larmor radius (FLR) effects are included taking an average over the gyroperiod. Poloidal sheared flows are included which are responsible for the creation of the transport barrier. For large wave amplitudes, widespread chaos dominates the phase space interrupted only by the most stable KAM surfaces. The torus breakup depends on the values of the parameters of the map: wave amplitude A, flow velocity C and the Larmor radius ρ. For two types of sheared poloidal flows, having monotonic and non-monotonic shear, phase diagrams for barrier breakup are obtained by following the iterations of two points on either side of the barrier until the trajectories get mixed. The threshold that delimits the barrier breakup has the typical feature of a fractal curve for all phase diagrams.

ARTICLE HISTORY
Received 30 November 2021
Accepted 9 February 2022

KEYWORDS
Plasma transport; dynamical systems; Hamiltonian systems

1. Introduction

Hamiltonian systems are well suited to describe several problems in plasma physics such as heating by waves or anomalous transport in magnetically confined plasmas. In particular, the turbulence produced by small-scale fluctuations that produce non-collisional transport can be studied using the chaotic behavior of a Hamiltonian system describing wave-particle interactions. Providing the power spectrum of the waves, the dynamics of the interaction can give rise to chaos which produces the particles to move in seemingly random trajectories which are sometimes described as Lagrangian turbulence. The analysis can be usually simplified by reducing the differential equations of the Hamiltonian system to a discrete map since this reduces the computing time considerably. Chaos in symplectic maps has been studied extensively (*1*) revealing many interesting properties that can relate to turbulent particle transport.

In the transition from regular to chaotic motion in symplectic maps, regular surfaces are destroyed giving way to chaotic regions bounded by stable KAM torii until a state is reached

CONTACT Julio J. Martinell martinel@nucleares.unam.mx

where global chaos is established. The last surviving KAM torus is commonly identified with a transport barrier. When global chaos sets in, particles can travel unimpeded through phase space giving rise to transport with specific properties that depend on the characteristics of the map. For some type of wave frequency spectrum, the map derived from the Hamiltonian system is exact (*2*) and can be used to get precise results for stochastic transport. This map is similar to the one describing stochastic plasma heating by lower-hybrid waves (*3*) and is a special case of the kicked Harper map which has been used to study anomalous diffusion (*4*, *5*) and transport barriers (*6*).

An important effect in fusion plasmas is the presence of seared flows since they have been shown to stabilize various instabilities and may produce a concomitant turbulence reduction. It is therefore of interest to include a sheared flow in the map which is linked to new KAM torii representing the particle trajectories carried by the plasma flow (*7*). When chaos becomes widespread the last KAM surface to break up acts as a transport barrier separating chaotic regions and preventing particles from diffusing from the center to the plasma edge. The determination of the barrier breakup conditions is quite important since it gives the parameters for the plasma to be well confined. The purpose of this paper is to determine these conditions for two different kinds of flows: those that vary monotonically with the transverse distance (shear of one sign) and those having a non-monotonic variation (shear changing sign).

Depending on the nature of the map the transport barriers have different properties. For non-degenerate maps (when the rotation number has a non-vanishing derivative), also known as twist maps, the last KAM surface to break up is the one with the most stable irrational rotation number (usually the golden mean). For non-twist maps which violate the non-degeneracy condition the most robust torus is the shearless surface. When there are no background plasma flows, transport barriers are not a characteristic feature of the map, although in (*6*) they were characterized for the kicked Harper model. However, the presence of flows produces clear transport barriers since the flow lines give rise to KAM torii that are resilient to chaos.

Transport barriers have also been studied with a Hamiltonian system that includes particle interaction with just two waves, by directly integrating the equations of motion (*8*, *9*). The barrier breakup diagrams obtained were found using the indicator points method (*10*), which is applicable to non-twist maps, providing a reliable way for the determination of the parameters for good plasma confinement. The use of a mapping adopted here makes computations faster allowing a more convenient way of computing barrier breakup diagrams. However, since we consider both twist and non-twist mappings we use a method applicable in the two cases. Otherwise, separate formal methods should be considered since for non-twist maps KAM theory does not apply and different approaches have been developed for their study (*11*). Here, as well as in (*8*, *9*), there is an emphasis on FLR effects.

The paper is organized as follows. In Section 2 the wave-particle model adopted is briefly described including the FLR corrections. The properties of the map without macroscopic flow are summarized. Then, in Section 3 the modification to the map by a macroscopic poloidal flow is introduced describing the use of monotonic and non-monotonic flows. Section 4 describes the method for analyzing barrier breakup and the phase diagrams are shown and discussed in Section 5 for both flow types. Finally, the conclusions are presented in Section 6.

2. Transport model

For a test particle moving in the magnetic field of a toroidal plasma (assumed in the z direction) subjected to an n electrostatic potential $\phi(x,y)$, the guiding center motion can be written as a Hamiltonian system

$$\frac{\mathrm{d}x}{\mathrm{d}t} = -\frac{\partial\phi}{\partial y}, \quad \frac{\mathrm{d}y}{\mathrm{d}t} = \frac{\partial\phi}{\partial x},$$

which can be averaged over gyro-radius to take into account the finite Larmor radius effects, using

$$\langle\Psi\rangle_\theta \equiv \frac{1}{2\pi}\int_0^{2\pi} \Psi\left(x+\rho\cos\theta, y+\rho\sin\theta\right)\mathrm{d}\theta.$$

It has to be pointed out that in this slab model the coordinates (x,y) correspond to radial and poloidal coordinates respectively in the torus. For an infinite, discrete wave spectrum of the form

$$\phi = A\sum_{n=-\infty}^{\infty}\cos(x+\theta_n)\cos(y+\theta_n-nt). \tag{1}$$

the equations can be exactly converted into a discrete map, which after gyro-averaging takes the form (7)

$$\begin{aligned} x_+^{n+1} &= x_+^n + 2\pi A J_0(\sqrt{2}\rho)\sin(x_-^n) \\ x_-^{n+1} &= x_-^n - 2\pi A J_0(\sqrt{2}\rho)\sin(x_+^{n+1}) \end{aligned} \tag{2}$$

where $x_\pm = x \pm y$ and $J_0(x)$ is the Bessel function of zero order.

This map is a special case of the kicked Harper model for the case of equal amplitudes of the sinusoidal, which has been studied extensively (3, 4). The phase-space structure has periodic closed particle orbits that are local KAM torii, which become chaotic around the hyperbolic points as the amplitude A is increased. The chaotic region increases until the phase space becomes totally chaotic for large enough A. The Larmor radius has the effect of reducing the chaotic regions size (7) implying that high-energy particles have less transport than thermal particles (see Figure 1). This is a non-twist map since the non-degeneracy condition $\partial x_-^{n+1}/\partial x_+^n = 0$ is violated for $x_+^{n+1} = (2j+1)\pi/2$. This defines a shearless curve.

In Figure 1 it can be appreciated that for large A chaos connects the left-hand side of the space (the plasma core) with the right-hand side (plasma edge) which amounts to having bad particle confinement. For $A \gg A_c = 0.318/J_0(\sqrt{2}\rho)$ there is global chaos in phase

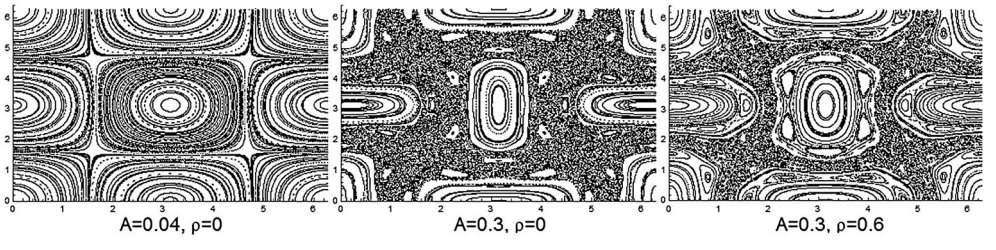

Figure 1. Phase-space diagram for the particle orbits with $A = 0.04, 0.3$; $\rho = 0, 0.6$.

space and particles are transported in random walk-like trajectories. It can be shown that the transport is diffusive with a quasilinear diffusion coefficient proportional to the squared amplitude $D \sim A^2$ (2, 7). The overall transport can be modified by the presence of accelerator modes which are stable periodic orbits that coherently propagate across the phase space. For the kicked Harper map it has been shown that they produce a divergence in the diffusion coefficient and they can induce partial transport barriers, or cantori, in the chaotic regions which modify the nature of the transport to be superdiffusive (5). However, for this special case, there are no transport barriers of relevance since in spite of the existence of a shearless curve it is broken up before global chaos is established (6).

3. Inclusion of poloidal flows

A macroscopic poloidal flow along y direction can be included adding an AC component to the electrostatic potential representing a radial electric field. The resulting map is a composition $\mathbf{M} = \mathbf{T}_2 \cdot \mathbf{T}_1$ of the following single maps

$$\mathbf{T}_1 : \begin{cases} x'_+ = x^n_+ + \pi\,\Omega(x^n) \\ x'_- = x^n_- + 2\pi A J_0(\sqrt{2}\rho)\sin(x'_+) - \pi\,\Omega(x^n) \end{cases} \tag{3}$$

$$\mathbf{T}_2 : \begin{cases} x^{n+1}_- = x'_- - \pi\,\Omega(x') \\ x^{n+1}_+ = x'_+ - 2\pi A J_0(\sqrt{2}\rho)\sin(x^{n+1}_-) + \pi\,\Omega(x') \end{cases} \tag{4}$$

where $\Omega(x)$ is the flow velocity profile.

Depending on the form of function $\Omega(x)$ the flow can be monotonic or non-monotonic. When $\Omega(x)$ is linear the composite map $\mathbf{M}$ can be reduced to a single map that has a unitary Jacobian assuring that it is an area-preserving or symplectic map. For $\Omega(x) = Cx$, in the explicit form it becomes

$$x^{n+1}_+ = x^n_+ + 2\pi A J_0(\sqrt{2}\rho)\sin(x^n_-) - \frac{C}{2}(x^n_+ + x^n_-) \tag{5}$$

$$x^{n+1}_- = \frac{1}{1 - C/2}\left[x^n_- - 2\pi A J_0(\sqrt{2}\rho)\sin(x^{n+1}_+) + \frac{C}{2}x^{n+1}_+\right] \tag{6}$$

In addition to the linear velocity profile, all variations that are monotonic in x have a non-zero derivative $\mathrm{d}\Omega/\mathrm{d}x$ which implies it is a twist map. On the other hand, if $\Omega(x)$ is non-monotonic, it has maxima or minima, where the derivative is zero. Thus the map can be non-twist when $\partial y^{n+1}/\partial x^n = 0$ for some set of points that would define a shearless curve.

It is of interest to study both types of profiles to compare the results, thus in addition to the linear velocity profile we consider a non-monotonic profile with a Gaussian dependence given by

$$\Omega(x) = Ce^{-x^2} \tag{7}$$

An important difference between the two profiles is that the linear type is finite over the whole space and has zero average velocity since it is symmetric over positive and negative values, whereas the Gaussian profile is localized over a finite range of x and has a net average velocity. The latter resembles the type present in plasmas with zonal flows and then it can be used to model that phenomenology that is quite common in toroidal plasmas. Although

there is more to the zonal flow phenomenon than just the profile shape, some of its features can be reproduced with this model. In particular, the appearance of a strong transport barrier has been associated with non-monotonic profiles located around the shearless curve in both rotating fluids and plasmas (*12*).

The phase-space structure when there is background flow includes global invariant tori that extend along the flow direction. Some of the most stable torii may have the effect of transport barriers when chaos starts developing. For the linear flow, depicted in Figure 2 the structure is not modified close to $x = 0$ because there the velocity is small but farther away from the streamlines that carry the particles with the flow are dominant when the wave amplitude and the flow velocity are small. When chaos starts spreading these curves do not allow a communication from the center to the edge, as seen in the two right panels of Figure 2. The radial transport is thus hindered by the KAM tori. Only when they are destroyed, as global chaos is established, transport can be effective in taking particles to the plasma edge. This happens as A increases but also when C gets larger.

The streamlines that cross from top to bottom in Figure 2 are the invariant KAM tori which are identified by a rotation number. According to KAM theory, the torii with rational rotation numbers are destroyed first and the most robust are those with irrational rotation numbers. A transport barrier will subsist until the last KAM torus is destroyed. In the next section, we describe how the destruction is determined.

For the non-monotonic flow, the phase space is mainly affected around $x = 0$, as opposed to the linear flow, since it is there where it is concentrated. This zonal flow then meanders about the central region and it is no longer symmetric and thus the figure depicts the positive and negative region. When the flow strength C rises, it initially straightens the flow lines but when rising further it gives rise to chaotic regions. On the other hand, an increase in the wave amplitude A produces an increment in the level of chaos, as is usual. The shearless curve is embedded in the meandering flow and it is expected to be the last to survive to chaotic breakup (Figure 3).

The effect of FLR is always to reduce the chaotic regions size and so it is expected that for larger Larmor radii the transport barrier breakup would be delayed. Visually, it is sometimes not so clear the chaos reduction effect of the FLR, especially when global chaos is established, but it can be assessed by computing the Lyapunov exponents when ρ is changed since this gives a measure of the level of chaos. This computation can be done in a way similar to that in (*13*). When this is done for the two types of flow it was found, as an example, that (a) in the linear profile for the parameters $A = 0.2$, $C = 0.75$ the Lyapunov exponents

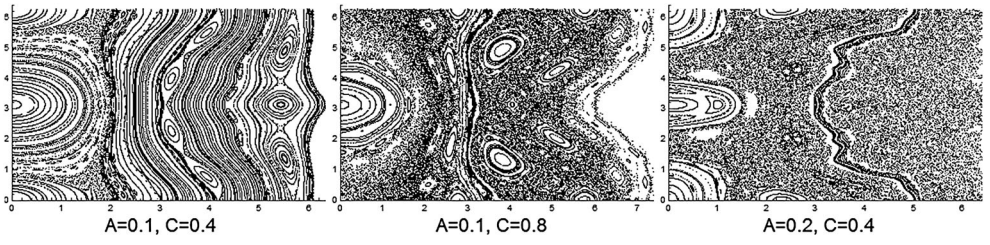

Figure 2. Phase space of particle orbits with linear flow with $\rho = 0$ for values of $A = 0.1$, 0.2 and $C = 0.4, 0, 8$.

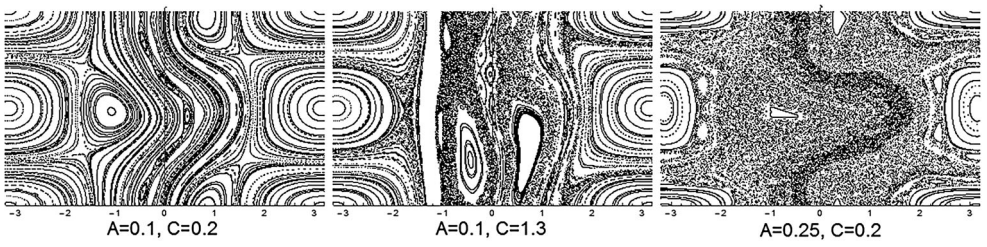

Figure 3. Phase space depicting the orbits in presence of flow with a Gaussian profile with $\rho = 0$ for values $A = 0.1, 0.25$ and $C = 0.2, 1.3$.

for $\rho = 0$ and $\rho = 0.2$ are $\lambda = 0.408$ and $\lambda = 0.399$, respectively and (b) in the Gaussian profile for the parameters $A = 0.2, C = 0.3$ the Lyapunov exponents for $\rho = 0$ and $\rho = 0.2$ are $\lambda = 0.193$ and $\lambda = 0.183$, respectively. In both cases, the reduction in λ when ρ increases indicates a reduction in the level of chaos. In addition, the level of chaos is lower in the Gaussian flow, for which the flow strength was taken smaller. Thus, for the same wave amplitude, larger flow shear produces more transport.

4. Determination of barrier breakup

Now we have to establish a way of finding the conditions for transport barrier breakup. There are several methods that have been developed for twist and non-twist maps. For the former case, some methods include criteria like Chirikov resonance overlap or Greene residue theorem which allow to find the parameter threshold values for the establishment of global chaos and hence barrier destruction (*1*). For non-twist maps, for which the standard KAM theory is not applicable, it is known that the most robust surface is located by the velocity maximum, where the shear vanishes (*11*). The level of chaos needed for its destruction can be determined using established methods for this situation such as the indicator points (*10*).

However, the application of these methods is cumbersome and dependent on the specific kind of map. In our case, it is sometimes not known a priori if the map is twist or non-twist, specifically for the non-monotonic profile. Therefore, we followed a method that is equally applicable for any situation having a transport barrier, although it is less formal than the others.

The first step is to locate the position of the barrier for a relatively low level of chaos. This is done by inspecting the phase-space diagrams. As an example, Figure 4 shows a few typical cases for the flow with a Gaussian profile. In red, there is the trajectory of a single particle with chaotic motion and in blue the trajectory of a second particle started in a different region. Since panels (a) and (c) they remain in separate regions this is indicative that there is a transport barrier between them that prevents the mixing of the two chaotic regions. In panel (a) there is a central barrier whereas in (c) there seem to be also two side barriers that keep the orbits confined in narrow regions. In (b) and (d) the mixing of colored dots is indicative that the central barrier has been broken although in (d) the side barriers are still present. The study presented here focuses on the existence of the central barrier which is expected to be the most robust, as mentioned before. For the linear profile, there is a similar situation although sometimes the location of the barrier is not so clear cut. In that

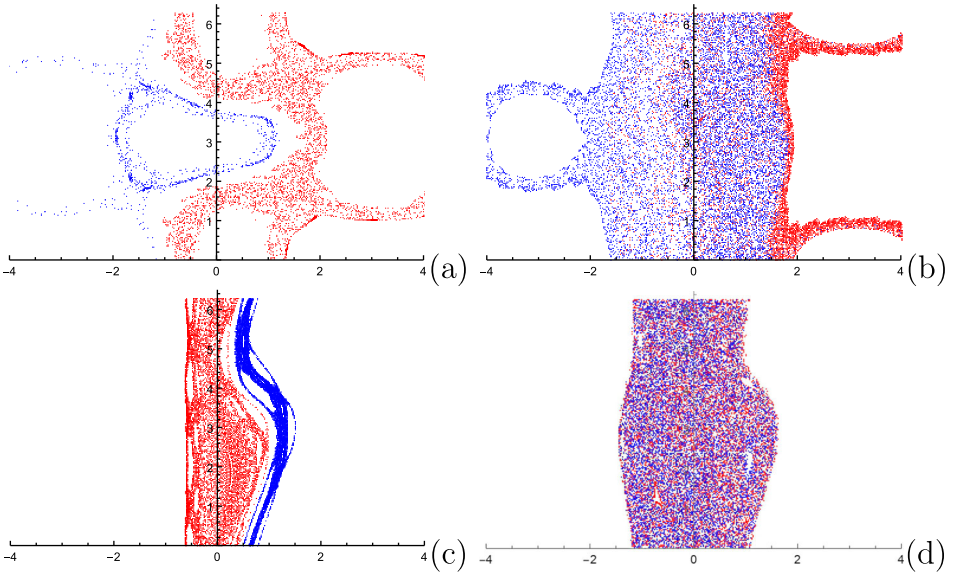

Figure 4. Phase space for two cases with local chaos separated by transport barriers and the concomitant disappearance. (a) Presence of a central barrier, (b) no barrier present, (c) central and side barriers and (d) central barrier broken remaining only side barriers.

case, there are no multiple barriers because the profile is not degenerate avoiding multiple resonances.

Once the barrier is located an ordered search is started for the threshold parameters that make the barrier break up. We start from a set of parameters (A, C, ρ) that allow a barrier and let two colored particles on each side of the barrier to evolve iterating the map 10^4 times. A scan is performed that varies each parameter in small steps across an interval leaving the others constant, generating the corresponding phase space diagrams. A visual examination of all the diagrams allows to determine the points for which the particle trajectories start to interpenetrate, marking the break up of the barrier. In some cases, there can be resurgences *i.e.* when the barrier disappears for a critical value of a parameter, say $A = A_{th}$, it can appear again for some $A > A_{th}$. The method we used has to be applied with care since sometimes it may appear that the barrier is present but when the number of iterations is increased there is an apparent barrier penetration. This is maybe due to the presence of cantori surfaces that are semi-permeable and they are not real barriers. Therefore, once a possible threshold value has been found, the number of iterations should be increased to make sure it still holds the particles. We can say that our computations are accurate up to the 10^4 iterations used.

5. The barrier breakup phase diagrams

Following the method described above, phase diagrams for the transport barrier breakup were generated for the relevant variables of the map, namely, A, C and ρ. This is the usual way to represent the behavior of barrier integrity in chaotic maps by showing the breakup threshold in two-dimensional diagrams. The two profile types are considered separately.

5.1. Monotonic velocity profile

The linear profile has a constant shear that produces KAM surfaces with progressively increasing rotation numbers, with rational and irrational values. The irrational surfaces survive longer and our method should isolate the most stable surface and determine the moment it breaks up, which is when global chaos sets in. This is the typical behavior of twist maps. In this case, the transport barrier was found to be located in the position shown in Figure 5.

In applying the breakup method, initial conditions for two particles on both sides of the barrier were given and the parameters were scanned in the ranges: A from 0.1 to 0.3 with step size $\Delta A = 0.005$; C from 0 to 0.9 with step $\Delta C = 0.001$; and $\rho = 0, 0.1, 0.2$. This gives a total of 110,700 states. The resulting phase diagram in $A-C$ space for constant $\rho = 0$ is shown in Figure 6. The colored area is where the barrier is no longer present while in the white area the barrier is stable. As is usually the case in the phase diagrams, the threshold boundary is irregular with jagged features which have made it to be called 'bird wing diagram '. Actually, it has been shown that the boundary is not a 1D curve but a fractal. The general tendency is that for large A or C the barrier is broken. The jagged structure of the boundary reflects the phenomenon of barrier resurgence mentioned before. For a fixed value of A, the increment of C may lead to destruction of the barrier and then to a reappearance when$C$ increases more (like in $A = 0.18, C = 0.34, 0.35$).

FLR effects are seen in Figure 7 where the same A vs. C diagrams are shown but for the other two values of ρ considered. Due to the smallness of the Larmor radius, the differences are not large but upon close examination, it can be seen a small shift to the right in some of the features which would be indicative of a longer duration of the barrier as ρ increases. The reason for using these small values of ρ is that, in normalized units, that is what corresponds to thermal particles in a typical tokamak plasma.

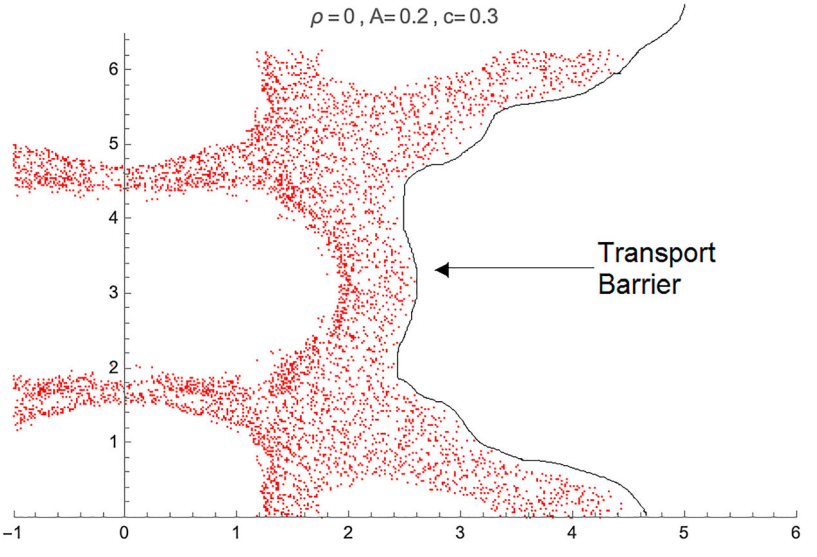

Figure 5. Transport barrier for the monotonic linear flow marked with black line. A particle chaotic orbit is held by the barrier on one side.

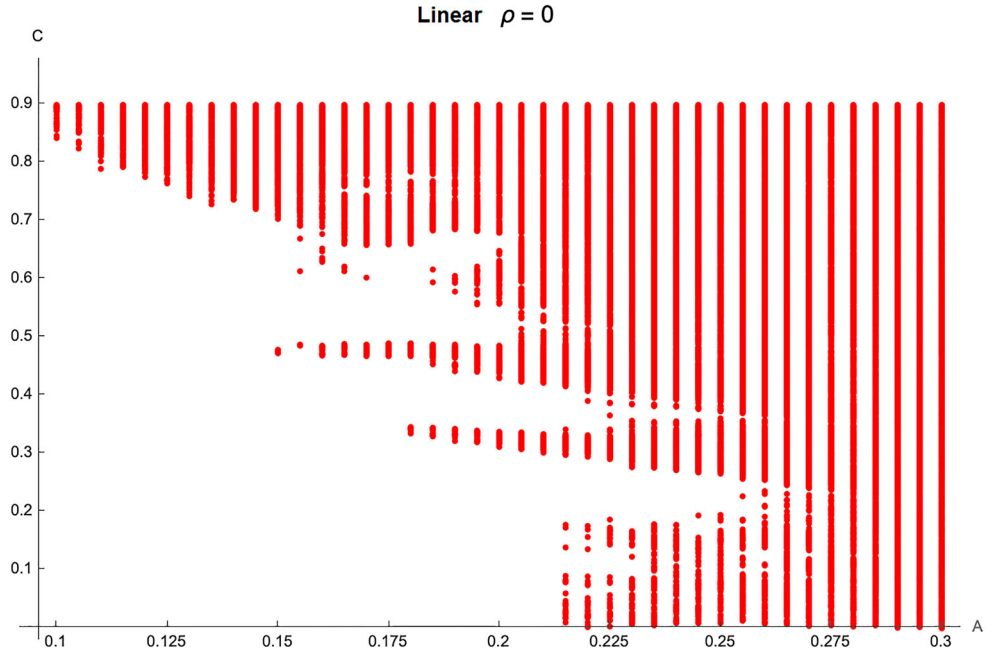

Figure 6. Breakup diagram in $A-C$ space for constant $\rho = 0$ for the linear profile. White regions are where a barrier is present.

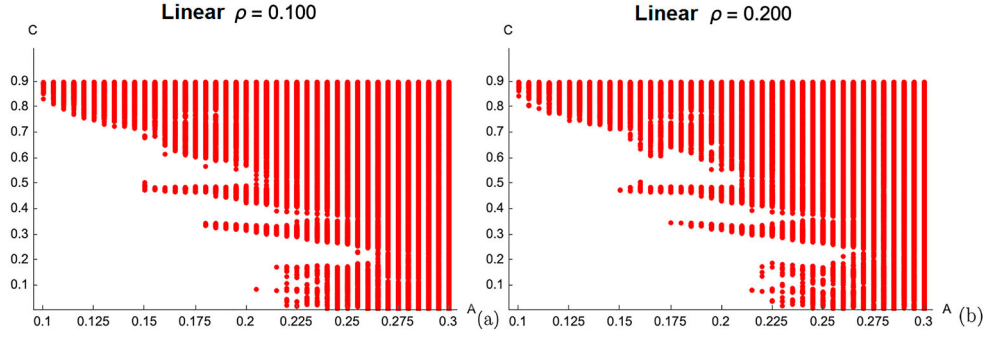

Figure 7. Breakup diagrams in $A-C$ space for two values of ρ for the linear profile. White regions are where a barrier is present.

5.2. Non-monotonic velocity profile

For non-monotonic flows, the map can be non-twist, in which case the criterion for barrier breakup is related to the robustness of the shearless curve. These barriers are more robust than in twist maps. The location of the barrier for the Gaussian profile given in Equation (7) is shown in Figure 8. Applying the same method as before, the two particles are initiated on each side of this barrier, letting them evolve for 10^4 iterations. The parameter scan is performed within the following ranges: A from 0.1 to 0.3 with step size $\Delta A = 0.005$; C from 0 to 2 with step size $\Delta C = 0.001$; and as before $\rho = 0, 0.1, 0.2$. This time the total number of

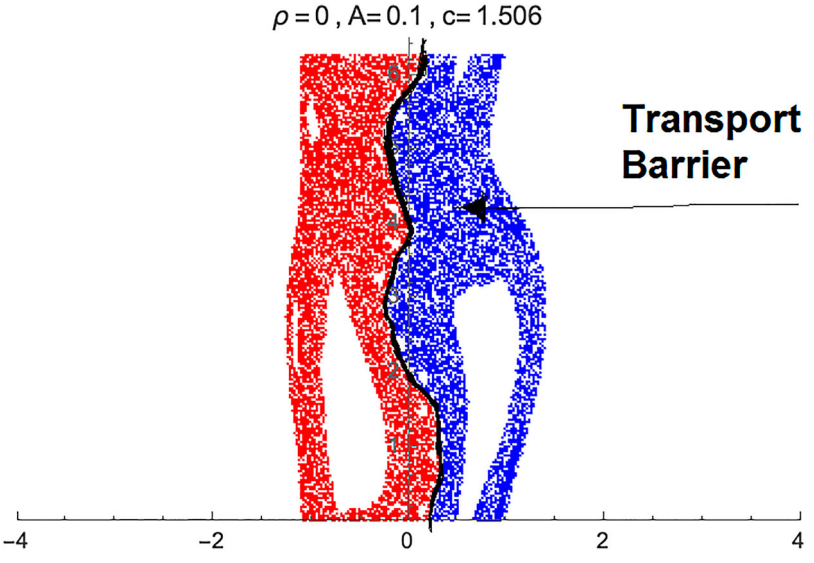

Figure 8. Transport barrier for the non-monotonic Gaussian flow marked with black line. Chaotic orbits of two particles (blue and red) are kept separated by the barrier.

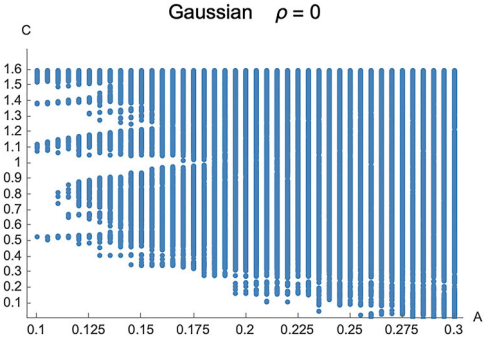

Figure 9. Breakup diagrams in $A-C$ space for constant $\rho = 0$ for the Gaussian profile. White regions are where a barrier is present.

states is 246,000. The resulting phase diagram in $A-C$ space for the case of $\rho = 0$ is shown in Figure 9.

Again, the white area is where the barrier is still present. It is noticed that for this case the barrier persists for larger values of the flow C, and at some points, it extends to large A values. This is indicative of the higher robustness of the barrier. For other values of the Larmor radius, the structure is almost the same as seen in Figure 10 although there is a small increment in the white region, especially for $\rho = 0.2$, as in the linear case, indicating the stabilizing effect of FLR.

For energetic particles, the stabilizing effect of FLR should be more important keeping the transport barrier for larger values of the parameters A and C. This effect is clearly seen in Figure 11 where the phase diagram of $\rho - C$ is presented for a value of $A = 0.5$. For this diagram, a scan over ρ was run from 0 to 2.7 in steps of $\Delta\rho = 0.025$ while C was varied from

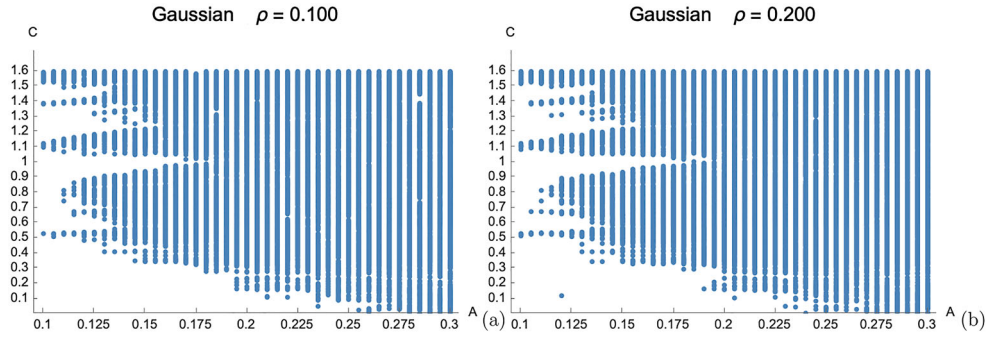

Figure 10. Breakup diagrams in $A-C$ space for two values of ρ for the Gaussian profile. White regions are where a barrier is present.

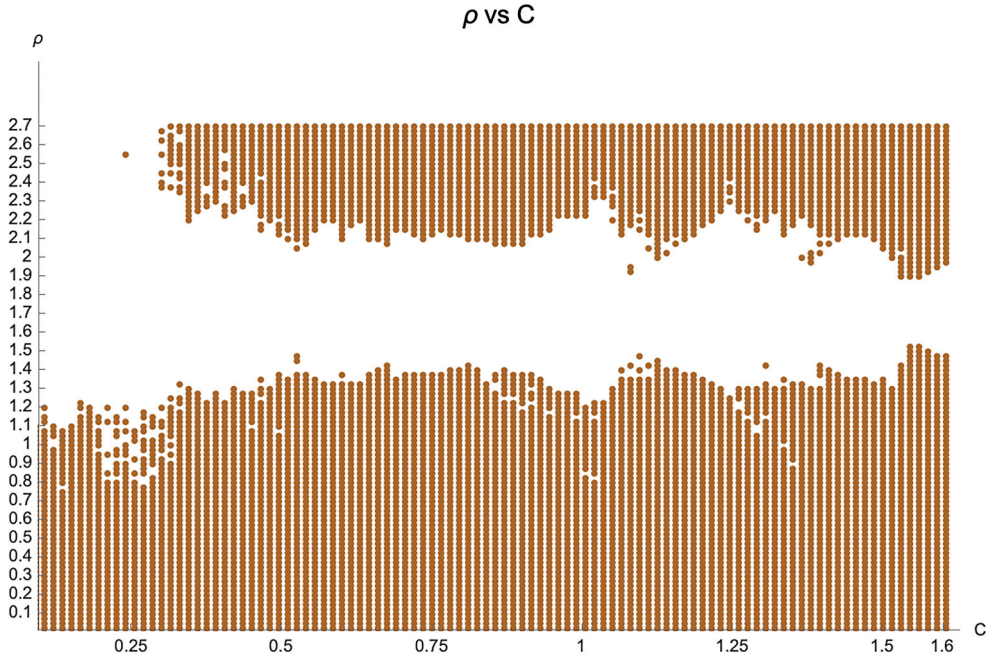

Figure 11. Phase diagram for ρ vs. C when $A = 0.5$ which corresponds to global chaos. Barrier is reestablished when ρ is close to a zero of $J_0(\sqrt{2}\rho)$.

0.015 to 1.605 with the step $\Delta C = 0.015$. The value of A was chosen so that the system is completely chaotic for all values of C. Then the stabilizing effect of FLR is seen when the barrier appears as ρ is increased over 1, although larger values are needed for large C. This effect is the result of the way ρ enters in the map which is multiplying the amplitude A by the Bessel function $J_0(\sqrt{2}\rho)$. Then, when the Bessel function is close to zero the effective wave amplitude is small and the chaos is much reduced. For the same reason, the barrier gets destroyed again when ρ increases further beyond the zero of $J_0(x)$.

6. Conclusions

The transport barriers due to the presence of sheared flows in a plasma in combination with drift waves in two dimensions have been analyzed. Plasma wave interactions are modeled by a guiding center approach of test particles with FLR corrections. The description is reduced to a symplectic iterative map which is used to follow the evolution of an ensemble of particles in an efficient way. The chosen wave spectrum (Equation (1)) leads to a map that is a particular case of the well known kicked Harper model, which leads to chaotic orbits when the wave amplitude A is increased. The resulting diffusive transport scales like $D \sim A^2$. FLR effects reduce the level of chaos. When the shear flow is added, the map is modified by the appearance of integrable KAM surfaces that run along the flow direction. These surfaces do not let the chaos propagate to cover all phase space and thus act as transport barriers.

The plasma flow represents the poloidal flows that are common in toroidal plasmas. Two types of shear flow profiles have been considered having qualitative different properties: (a) a monotonic variation with radius and (b) a non-monotonic variation which is localized to a finite region of the plasma and has a maximum value at some radius. The former is taken here as a linear flow, while the latter is represented by a Gaussian function and may be considered as a simple model for a zonal flow (although the full concept of a zonal flow is more extensive). In both cases, the associated transport barriers were characterized indicating that, in the linear flow the description corresponds to a twist map while the Gaussian flow may produce a non-twist map. The transport barrier for the twist map is the last KAM surface to break up. In the non-twist map, the transport barrier is associated with the shearless surface which is quite robust. After identifying the location of the transport barriers in each case, their integrity of them was analyzed with a method that follows two particles on each side of the barrier. When their trajectories get mixed, it marks the destruction of the barrier. With this method, phase diagrams have computed that show the boundary of the barrier breakup in the $A-C$ space. The boundary has the typical bird wing shape indicating the presence of barrier resurgences. As a general feature, the barriers break up when either A or C are raised enough.

While the method applied here is not very accurate and the resolution of the diagrams is relatively low, they give pretty good information on how the behavior of the barriers is in these maps. Also, FLR effects were noted in the sense of reducing the loss of particles and in delaying the destruction of the transport barrier. For both profile types, the results are similar although for the Gaussian flow they seem to be more resilient, in agreement with what is expected in non-twist maps.

Since transport barriers are extremely important for fusion plasmas, the results presented here are quite relevant to the understanding and advancement of plasma confinement. In particular, our results indicate that the velocity shear, while needed for barrier formation, should not be made too large because that would destroy the barrier. Our results should be improved by applying more accurate methods for barrier destruction such as the Chirikov resonance overlap of the Greene's residue criterion (*1*). For non-twist maps, there are other methods like the indicator points which are based on the symmetries of the map (*10*).

Disclosure statement

No potential conflict of interest was reported by the author(s).

Funding

This work was partially supported by project DGAPA-UNAM IN110021 and by Conacyt project A1-S-24157. Support from supercomputer project LANCAD-UNAM-DGTIC-104 is also acknowledged.

Notes on contributors

Carolina A. Tafoya has BS in Physics from National Autonomous University of Mexico (UNAM).

Julio J. Martinell has a PhD from MIT, USA and is a Professor at Instituto de Ciencias Nucleares, UNAM.

References

(1) Lichtenberg, A.J.; Lieberman, M.A. *Regular and Chaotic Dynamics*, 2nd ed.; Springer: New York, 1992.
(2) Kleva, R.; Drake, J. *Phys. Fluids* **1984,** *27,* 1686.
(3) Karney, C.F.F. *Phys. Fluids* **1979,** *22,* 2188–2209.
(4) Saito, S.; Nomura, Y.; Ichikawa, Y.H. *Prog. Theor. Phys.* **1995,** *94,* 745.
(5) Leboeuf, P. *Phys. D* **1998,** *116*, 8–20.
(6) Shinohara, S. *Phys. Lett. A* **2002,** *298*, 330–334.
(7) Kryukov, N.; Martinell, J. J.; del-Castillo-Negrete, D. *J. Plasma Phys.* **2018,** *84*, 905840301.
(8) Martinell, J. J.; del-Castillo-Negrete, D. *Phys. Plasmas* **2013,** *20*, 022303.
(9) del-Castillo-Negrete, D.; Martinell, J.J. *Commun. Nnlinear Sci. Numer. Simul.* **2012,** *17*, 2031–2044.
(10) Shinohara, S.; Aizawa, Y. *Prog. Theor. Phys.* **1997,** *97*, 379.
(11) del-Castillo-Negrete, D.; Greene, J.M.; Morrison, P.J. *Phys. D* **1996,** *91*, 1.
(12) del-Castillo-Negrete, D.; Morrison, P.J. *Phys. Fluids A* **1993,** *5*, 948.
(13) Ramasubramanian, K.; Sriram, M.S. *Phys. D* **2000,** *139*, 72–86.